Chapter

Toward UWB Impulse Radio Sensing: Fundamentals, Potentials, and Challenges

Jonas Ninnemann, Paul Schwarzbach and Oliver Michler

Abstract

Radio sensing is a rapidly emerging research field. It focuses on designing an integrated communication system that can also perform localization and radar functionalities sharing the same transmit signals and potentially the same hardware. Ultra-wideband (UWB) impulse radio is a promising technology for radio sensing because it offers a high-range resolution and direct access to the channel impulse response (CIR) to observe the multipath components (MPCs) of the wideband channel caused by scattering at target objects. This approach enables a wide range of functionalities and applications, especially in the field of mobility and transportation. The foundation is given by the signal propagation and channel modeling of the UWB channel, which is briefly revisited in this chapter. Based on the CIR and estimated MPCs the target object can be localized like a multistatic passive radar. The influence of geometry in a passive target localization system is studied by calculating the geometric dilution of precision (GDOP). In addition to passive localization more tasks and functionalities of radio sensing, are briefly introduced including detection, tracking, imaging, counting, and classification. The chapter concludes with further research directions and challenges in UWB radio sensing, especially for real-world use in the context of mobility applications.

Keywords: multipath-assisted radio sensing (MARS), channel model, channel impulse response (CIR), multipath components (MPCs), impulse radio (IR), radio sensing for intelligent transportation systems (ITS)

1. Introduction

Ultra-wideband (UWB) impulse radio (IR) is extensively researched and used as a technology for indoor positioning systems [1, 2] and short-range communication [3]. Such systems are enabled by key features of the UWB physical layer (PHY) such as high bandwidth, the transmission of very short impulses, and low power. These features lead to a high range resolution and usually dense networks, which in general makes UWB perfectly suitable for radio sensing tasks and applications.

The term radio sensing first emerged in the context of cellular networks and is referring to the usage of existing radio signals to passively sense the environment

[4–6]. The goal is to perform communication, localization, and radar functionalities by sharing the same transmit signals and potentially the same hardware. The analysis of the radio signal itself enables new features and functions of the communication systems such as localization, tracking, imaging, detection, or classification of passive target objects without the need for dedicated hardware or specialized measurement setups. In the past, this approach referred to UWB-IR and was mostly considered for tracking [7, 8], imaging [9], and people counting [10]. In contrast to such radar systems, radio sensing follows a more integrated approach by combining communication, localization, and sensing functionalities with the same radio signal and hardware to be more cost and spectrum efficient. This way the IR could be an integrated part of future communication networks to fulfill sensing tasks [5].

UWB and its IR nature allow direct access to the channel impulse response (CIR) in the time domain as the fundamental signal parameter for channel estimation. The CIR measurement includes information about the different propagation paths of the signal (direct path and echo paths). For passive target localization, the CIR is measured, and the multipath components (MPCs) are extracted to fulfill the different tasks of radio sensing. The high bandwidth of UWB ($\geq$ 500 MHz) allows the distinguishing of MPCs in the CIR, even if the time delay of the propagation paths is relatively close together [11].

There are many use cases of radio sensing ranging from smart cities, smart homes, vehicular networks, and health to drones. In terms of mobility applications, radio sensing based on UWB could be helpful and game-changing for intelligent transportation systems (ITS). **Table 1** lists possible use cases of radio sensing for the various modes of transport and tasks of radio sensing.

To implement the use cases, UWB is a promising technology for radio sensing. Therefore, this chapter transfers radio sensing approaches to UWB for different tasks and functionalities. In particular, the chapter provides the necessary fundamentals and proposes a UWB radio sensing approach based on the multipath channel model. Limitations in terms of range resolution and sensor arrangement are discussed, as well as further research directions and challenges.

The rest of this chapter is organized as follows: Section 2 gives an overview of the research field of radio sensing, the different scientific and technological influences, and the current state-of-the-art. In Section 3, the basics of signal propagation are introduced to derive the wideband multipath channel model. Based on this, a UWB radio sensing approach is then described in Section 4 for passive target localization. In addition, the influence of network geometry is investigated for different transceiver

Mode of transportation	Localization	Detection	Classification
Automotive	Vehicular networks and automotive radar	Parking lot occupancy detection	Automotive radar
Rail transport	Flow management in stations	Passenger detection on platforms or inside trains	
Aviation	Boarding monitoring	Seat occupancy detection	Classification of objects to automated passenger safety checks
Drones/UAVs	Landing system	Obstacle detection	Obstacle classification

Table 1.
Use cases of UWB radio sensing for intelligent transportation systems.

constellations and other tasks of radio sensing are briefly introduced. In Section 5 challenges and further research directions for UWB-based radio, sensing is discussed. The chapter concludes with a summary of the key contributions in Section 6.

2. Taxonomy of radio sensing

The research field of radio sensing is composed of different scientific directions and is only made possible by the fusion of these influences and ideas. The three main pillars are wireless communication systems, localization based on RF signals, and radar systems. The different terms and concepts in this highly interconnected research field are presented in a word cloud in **Figure 1**.

Wireless communication systems [12, 13] have been used not only for networking but also for the localization of devices for years now. Especially in the context of indoor positioning systems (IPS) [1, 2], where no global navigation satellite systems (GNSS) are available, localization enables new services and applications. To estimate the location of a mobile sensor (tag) a wireless sensor network (WSN) [1], consisting of fixed sensors (anchors) with known positions, is placed in the environment. Based on different channel parameters and positioning principles, the position of the mobile tag is estimated. Because the target object or user needs to wear an active sensor, this technique is referred to as active localization. UWB is one technology for such localization systems, perfectly suitable due to its high positioning accuracy.

The same radio signal used for active localization can also be analyzed to enable device-free passive localization (DFPL) [14, 15]. Here, the target object does not need to carry a sensor, but instead the position is estimated by evaluating different channel and propagation effects. DFPL is one possible task of a radio sensing system. But based on the use of wireless radio technology and channel estimation procedures, many tasks can potentially be accomplished. For example, detection of the target object, mapping of the environment, tracking, classification of different scenes or counting of objects and people.

In the past, such tasks were accomplished by dedicated radar systems with specific hardware, spectrum, and techniques for the measurement of radar parameters. In

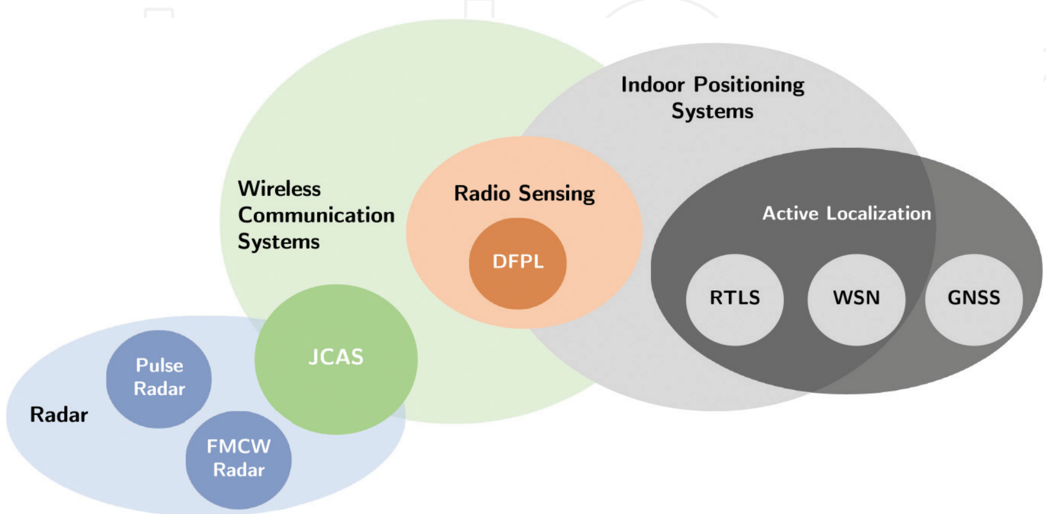

Figure 1.
Taxonomy of radio sensing as a fusion of different research directions in the context of integrated wireless communication systems. New abbreviations are joint communication and sensing (JCAS), frequency-modulated continuous wave (FMCW) radar, and real-time locating systems (RTLS).

principle, there are two different types of radars: continuous wave (CW) and pulse radar. One specific implementation of a CW radar is the frequency-modulated continuous wave (FMCW) radar. There are different geometrical configurations of radar systems such as monostatic, bistatic, or multistatic systems. The radar system can detect objects by transmitting a pulse or CW signal toward the target object and analyzing the reflected signal to estimate different signal parameters like the time-of-flight to the object [16].

More recent research focuses on the integration of these dedicated radar systems into cellular communication systems such as 5G/6G. The integration can be achieved through different levels starting from a better spectral coexistence of radar and communication systems over uniform hardware, RF frontend, and waveform design to true perceptive networks in the future. Different terms are used to describe such systems in research like Joint Communication and Sensing (JCAS) [5], Integrated Sensing and Communication (ISAC) [17], or radar communication (RadCom) [18]. This integration is only possible because of the trend to higher frequency spectrum and bandwidth in cellular networks and the resulting higher range resolution for sensing applications.

Paper	Channel parameter	Approach and algorithm	Task	Evaluation and use case
[19]	Amplitude and phase of the CIR	Multipath-assisted device-free localization	Mapping and localization	Simulation and measurements with DW1000[a]
[11]	CIR	Multipath-assisted radio tomographic imaging	Mapping and localization	Measurements with DW1000
[20]	MPCs	Multipath-enhanced device-free localization and Bayesian localization	Localization	Measurements with DW1000[a]
[21]	MPCs	Channel-SLAM with virtual transmitters	SLAM	Simulation
[7]	CIR	Background subtraction and particle filter	Real-time tracking	Measurements with DW1000[a]
[22]	Channel frequency response	Classification	Human activity recognition	Measurements with DW1000[a]
[23]	MPCs	Multipath-assisted positioning	Localization	Computational results
[24]	MPCs	Multipath-assisted navigation and tracking with PHD-filter	Multiple target tracking	Indoor UWB measurements
[25]	CIR and MPCs	Convolutional neural networks, particle filter	Passive human tracking	Measurements with DWM1000[a]
[26]	CIR	Clustering and Maximum Likelihood Equation	People counting	Measurements

[a] *DW1000 and DWM1000 is a UWB Transceiver IC and module from Qorvo [27].*

Table 2.
Different approaches and measurement principles for UWB radio sensing.

In terms of UWB, the IR is already part of the PHY concept. UWB sends very short pulses over a large bandwidth and uses pulse position modulation to transfer information. This concept enables active localization based on time of arrival estimation. Based on the transmitted pulses and the impulse response of the wideband channel, the PHY of UWB is perfectly suitable for different sensing tasks. In research, different approaches, algorithms, and use cases for UWB sensing are currently discussed (**Table 2**).

3. Signal propagation and channel model

3.1 Propagation phenomena

A radio communication system emits an electromagnetic wave, that experiences different propagation phenomena and effects before reaching the receiver (RX). In general, the energy of the radio signal is reduced in free space, where no obstacle is located between the transmitter (TX) and the RX (**Figure 2**). The Friis transmission model [28] stated that the received power P_r is given as follows [29]:

$$P_r = P_t G_t G_r \left(\frac{\lambda}{4\pi d}\right)^2 \tag{1}$$

where P_t is the transmitted power, G_t and G_r are the antenna gain of the TX and RX. The free-space path loss (FSPL) depends on the wavelength λ and traveled distance d of the signal.

In addition to the FSPL, the received power is further reduced, and the signal direction is influenced by three other basic propagation phenomena: reflection, diffraction, and scattering (**Figure 2**). These effects occur when the electromagnetic wave with wavelength λ encounters an object with size A. Reflections appear when the size of the object is very large compared to the wavelength: $A \gg \lambda$. The angle of the

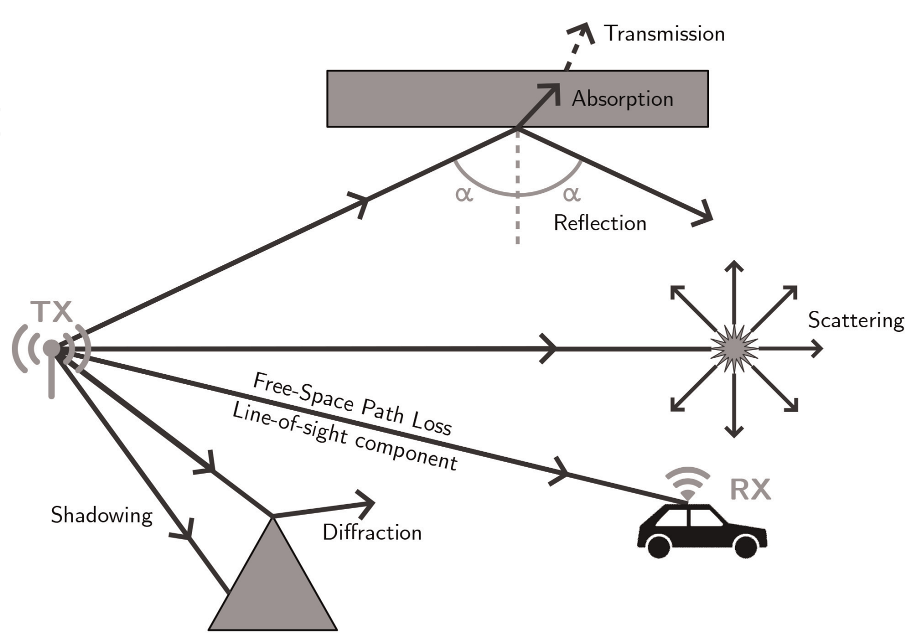

Figure 2.
Signal propagation and phenomena.

incident wave concerning the surface normal is equal to the angle that the reflected wave makes to the same normal. Reflections lead to a decrease in received power due to absorption or even the transmission loss of the wave energy by the encountered object. Diffraction arises when the wave hits an object with a size in the order of the wavelength ($A \approx \lambda$) and is explained by the Huygens principle. Scattering is the result of the encounter with a very small object compared to the wavelength: $A \ll \lambda$. Scattering occurs on objects with rough surfaces, whereby the incident wave is redirected in many directions [29, 30].

3.2 Channel effects

The wireless channel is affected and characterized by the variation of the channel strength or energy level over time and frequency. All effects combined are called fading, and the summarized attenuation of all effects is the path loss between the TX and the RX. Fading can mainly be categorized into large-scale fading and small-scale fading, according to **Figure 3**. Large-scale fading characterizes the variations in path loss over distance (FSPL, log-normal), and also shadowing (slow fading) or even blockage by large objects. These effects are typically frequency independent. Small-scale fading on the other hand describes the constructive or destructive interference of multiple signal paths between the TX and RX. This is caused by scattering and generally leads to a time-varying channel [13, 31, 32].

Especially small-scale fading must be considered for wideband channel models targeting sensing applications. Small-scale fading results in either a flat fading channel or a frequency-selective channel. The coherence bandwidth B_c is considered the bandwidth where the channel is regarded as a flat channel. This mean all signals passing through the channel experience similar attenuation and phase shifts. The root mean square (RMS) delay spread τ_{rms} is inversely proportional to B_c, which means larger τ_{rms} results in a more frequency selective fading channel. If the signal bandwidth B_s is higher than B_c the channel is considered a frequency selective fading channel. The time interval over which the wireless channel is constant is called coherence time T_c [29, 30].

3.3 Multipath propagation channel model

The path loss is the basis for empirical channel models, which model the received power at a reference distance according to the carrier frequency and the environment [29]. Empirical models consider different types of propagation environments and are

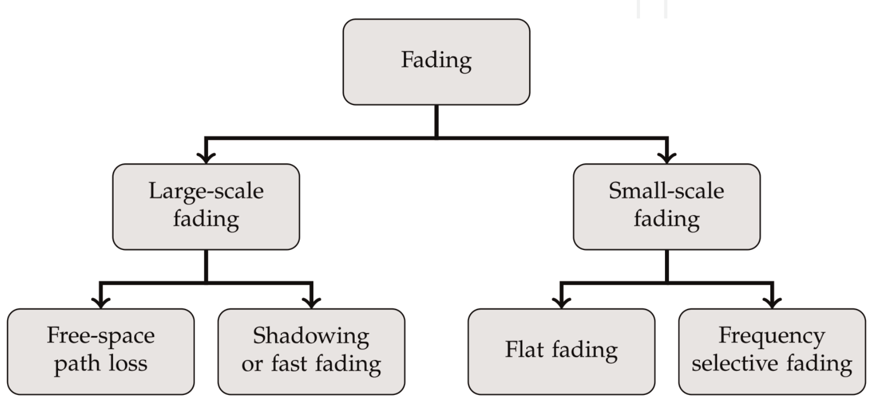

Figure 3.
Types of channel fading effects.

based on real-world measurements [33]. Flat fading channels are modeled with statistical models. For example, the Rayleigh fading distribution describes a statistical time-varying model for the propagation of electromagnetic waves. The Rice distribution modeling, a channel with one strong LOS component [29]. These models are based on measurements of the channel statistics for different predefined environment categories, but fail to resolve individual propagation paths. In comparison to statistical and empirical models, a deterministic model is more suitable for sensing approaches and applications. Individual propagation paths are calculated based on the aforementioned channel effects.

A multipath wideband frequency selective channel can be modeled as a linear time-varying system. We assume that the attenuation and propagation delay does not depend on the frequency inside the range of the coherence bandwidth of the channel. We can generalize the system to an arbitrary input $x(t)$ and compute the received signal $y(t)$ as follows:

$$y(t) = \sum_{i=1}^{N} a_i(t)x(t - \tau_i(t)) \tag{2}$$

where N is the number of different propagation paths with an attenuation $a_i(t)$ and propagation delay $\tau_i(t)$ at time t [13].

Because the channel is linear, it can be described by an impulse response $h(\tau, t)$ [13]. The CIR of a time-varying multipath channel is given as [29]:

$$h(\tau, t) = \sum_{i=1}^{N} a_i(t)\delta(t - \tau_i(t)) \tag{3}$$

where $a_i(t)$ and $\delta(t - \tau_i(t))$ is the attenuation, respectively, the delta function of the ith delayed propagation path. The Fourier-transformed impulse response of the system results in the following frequency response $H\ (f;t)$ in frequency domain f [13]:

$$H(f;t) := \int h(\tau, t)e^{-j2\pi f\tau}d\tau = \sum_{i=1}^{N} a_i(t)e^{-j2\pi f\tau_i(t)} \tag{4}$$

The fading multipath channel is now described by an input/output relation as an impulse response of a linear time-varying system. The system can be interpreted as a linear finite impulse response (FIR) filter and is also referred to as the tapped delay line model. An example of such an FIR-based channel model is illustrated in **Figure 4** with three different reflected paths and the LOS path, resulting in a four-tap FIR filter. Each tap corresponds to a reflected path with an amplitude $a_i(t)$ and a corresponding delay $\tau_i(t)$.

In a stationary case, where the $a_i(t)$ and $\tau_i(t)$ do not depend on time t we can model the channel as a usual linear time-invariant (LTI) system with the CIR corresponding to the following equation:

$$h(\tau) = \sum_{i=1}^{N} a_i\delta(t - \tau_i) \tag{5}$$

Multipath propagation causes different propagation effects depending on the propagation paths and shadowing. The direct path between the signal TX and RX is referred to as line-of-sight (LOS) propagation. In contrast, an obstructed or reflected

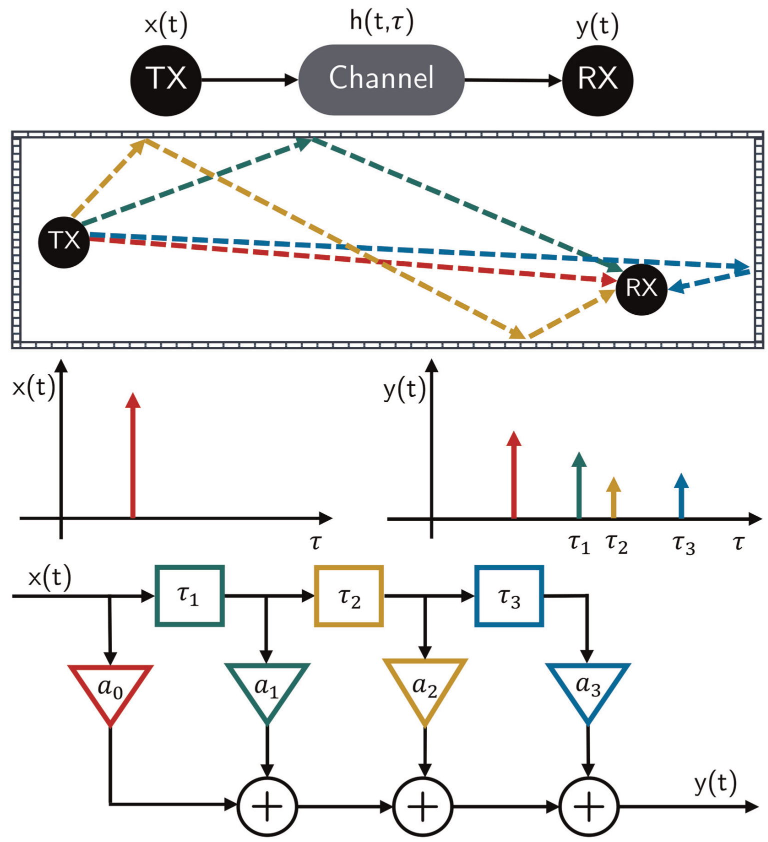

Figure 4.
Tapped-delay-line representation of the time-variant multipath channel model.

transmission path is called non-line-of-sight (NLOS). The term multipath reception applies if the signal reaches the RX via multiple paths caused by different propagation phenomena. This results in a received signal composed of attenuated, delayed, and phase-shifted replicas of the transmitted signal. These components can take different paths in the environment before reaching the RX and are thus called multipath components (MPCs) [30, 32].

3.4 Bandwidth and range resolution

The next step in channel modeling is to convert the time-continuous channel to a time-discrete channel with limited bandwidth B_s. In the case of UWB, the input waveform of the channel or transmitted signal is a Gaussian pulse with a certain pulse duration $T_d = \frac{1}{B_s}$ and a signal bandwidth of $B_s \geq 500$ MHz. The rectangular shape in the frequency domain corresponds in the time domain to the sinc function. Based on the sampling theorem we can sample the CIR following the Whittaker-Shannon interpolation formula [13]:

$$\tilde{h}(\tau) = \sum_{i=1}^{N} a_i sinc(B_s(t - \tau_i)) \tag{6}$$

where $sinc(\cdot)$ donates to the sinc function defined by $sinc(x) = \frac{sin\,(\pi x)}{\pi x}$. The sum of normalized sinc functions for every tap in the time-continuous signal allows the reconstruction of the CIR for the band-limited channel.

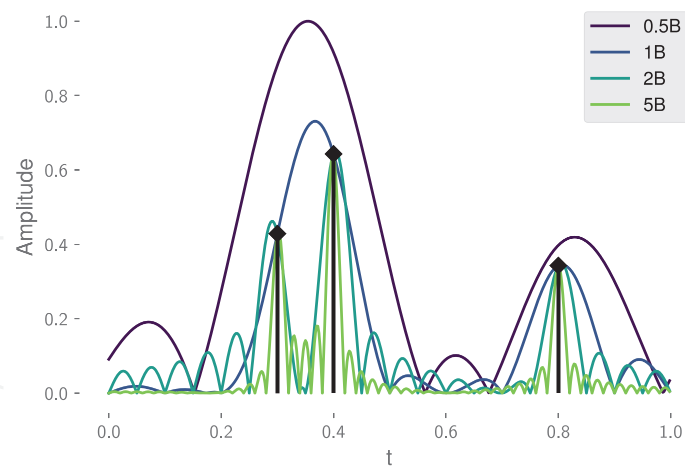

Figure 5.
Qualitative correlation between four different bandwidths and time resolution for bandlimited received signals: MPCs are marked as black Diracs and the signal is modeled as the sum of all sinc function according to Eq. (6). The axes are scaled with min–max scaling, as this is only a qualitative representation of the different bandwidths.

The argument of the sinc function in Eq. (6) is proportional to the used bandwidth. A larger signal bandwidth leads to a narrower sinc function. Thus, more individual MPC in the CIR can potentially be resolved [34]. Therefore, the achievable range resolution Δd for radio sensing is determined by the signal bandwidth B_s [35]:

$$\Delta d = \frac{c}{2B_s} \tag{7}$$

where c donates to the speed of light.

The range resolution is a key metric for many types of radio-sensing tasks and describes the ability to separate different MPC from each other in the CIR. **Figure 5** shows an example of a channel with three multipath components and the bandlimited reconstructed CIRs for different signal bandwidths. For the reconstruction, the signal is interpolated using a sinc kernel according to Eq. (6). The qualitative comparison of different bandwidths shows that a single MPC cannot be resolved if the bandwidth of the signal is not sufficient.

4. UWB radio sensing: Approach and tasks

4.1 Problem formulation

The channel model and impulse response from Eq. (5) can be translated into the spatial domain. The propagation delay τ_i of the ith MPC is the time the electromagnetic wave travels from TX, bouncing at the scatter point (SP) and arriving at the RX. The SP is located somewhere on the target object, which should be located or detected. The time can be converted to a distance d_i by multiplying with the speed of light c [36]:

$$d_i = \tau_i \cdot c = R_{\mathrm{TX,SP}} + R_{\mathrm{SP,RX}} + e_i \tag{8}$$

where $R_{\mathrm{TX,SP}}$ is the geometric distance between TX and SP, and $R_{\mathrm{SP,RX}}$ is the distance between SP and RX. The ranging error is represented by e_i. The measured distance d_i is the length of the propagation path between TX and RX.

For the target localization, we consider a wireless sensor network (WSN) with multiple sensor nodes. Now we can estimate kth different propagation delays $\tau_{i,k}$ for the different channels and also have different propagation path lengths $d_{i,k}$. We assume the WSN consists of an RX at position $\mathbf{X}_{\mathrm{RX}} = [0,0,0]^{\intercal}$ and $k = 1, \dots, K$ different TX at positions $\mathbf{X}_{\mathrm{TX},k} = \left[x_{\mathrm{TX},k}, y_{\mathrm{TX},k}, z_{\mathrm{TX},k}\right]^{\intercal}$. The SP at the target object is located at $\hat{\mathbf{X}}_{\mathrm{SP}} = \left[\hat{x}_{\mathrm{SP}}, \hat{y}_{\mathrm{SP}}, \hat{z}_{\mathrm{SP}}\right]^{\intercal}$ (**Figure 6**).

$$\begin{aligned} \boldsymbol{R}_{\mathrm{bi},k} &= \boldsymbol{R}_{\mathrm{TX}_k,\mathrm{SP}} + \boldsymbol{R}_{\mathrm{SP,RX}} \\ &= \sqrt{\left(x_{\mathrm{TX},k} - \hat{x}_{\mathrm{SP}}\right)^2 + \left(y_{\mathrm{TX},k} - \hat{y}_{\mathrm{SP}}\right)^2 + \left(z_{\mathrm{TX},k} - \hat{z}_{\mathrm{SP}}\right)^2} + \sqrt{\hat{x}_{\mathrm{SP}}^2 + \hat{y}_{\mathrm{SP}}^2 + \hat{z}_{\mathrm{SP}}^2} \end{aligned} \tag{9}$$

The bistatic range $\boldsymbol{R}_{\mathrm{bi},k}$ can be obtained or estimated for the measured propagation path $d_{i,k}$ and is then the sum of the transmitter-target range $\boldsymbol{R}_{\mathrm{TX}_k,\mathrm{SP}}$ and the target-receiver range $\boldsymbol{R}_{\mathrm{SP,RX}}$ according to the following equation: [37].

This is a non-linear optimization problem and therefore the solution is not directly obvious. One approach is iterative methods like the Taylor series linearization [38]. Another option is to estimate the target position by a closed-form solution [37, 39] like spherical-interpolation (SI) [40] or spherical-intersection (SX) [41].

4.2 Non-linear least squares estimation

To solve the non-linear equation system given in Eq. (9) the function is linearly approximated at a working point using Taylor's theorem. The solution of the resulting linear least-squares approach is used to adjust the position estimation in an iterative process [38, 42]. A first estimation of the target object position $\left(x_0, y_0, z_0\right)$ is utilized to initialize the Taylor series at this point. The innovation of this first estimation $\left(\delta_x, \delta_y, \delta_z\right)$ allows the adjustment of the estimation and is calculated as follows:

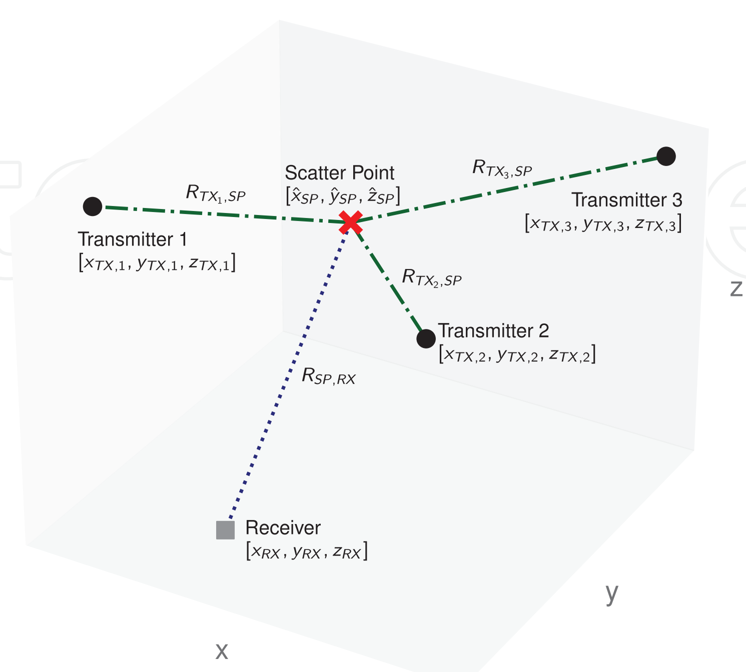

Figure 6.
The geometric configuration of the target and sensors for the localization.

$$\hat{x}_{\mathrm{SP}} = x_0 + \delta_x \qquad \hat{y}_{\mathrm{SP}} = y_0 + \delta_y \qquad \hat{z}_{\mathrm{SP}} = z_0 + \delta_z \tag{10}$$

The first-order Taylor polynomial T_k is used to calculate the linear approximation of Eq. (9) at the first estimation of the target object position:

$$\begin{aligned} T_k &= \boldsymbol{R}_{\mathrm{bi},k} + a_{k,x}\delta_x + a_{k,y}\delta_y + a_{k,z}\delta_z \\ &\approx \boldsymbol{R}_{\mathrm{bi},k}(x_0, y_0, z_0) + \left.\frac{\partial \boldsymbol{R}_{\mathrm{bi},k}(x,y,z)}{\partial x}\right|_{x=x_0,y=y_0,z=z_0}\delta_x + \left.\frac{\partial \boldsymbol{R}_{\mathrm{bi},k}(x,y,z)}{\partial y}\right|_{x=x_0,y=y_0,z=z_0}\delta_y \\ &\quad + \left.\frac{\partial \boldsymbol{R}_{\mathrm{bi},k}(x,y,z)}{\partial z}\right|_{x=x_0,y=y_0,z=z_0}\delta_z \end{aligned} \tag{11}$$

where $a_{k,x}, a_{k,y}$, and $a_{k,z}$ are the partial derivatives of the Eq. (9):

$$\begin{aligned} a_{k,x} &= \frac{x_{\mathrm{TX},k} - x_0}{\sqrt{(x_{\mathrm{TX},k} - x_0)^2 + \left(y_{\mathrm{TX},k} - y_0\right)^2 + (z_{\mathrm{TX},k} - z_0)^2}} + \frac{x_0}{\sqrt{x_0^2 + y_0^2 + z_0^2}} \\ a_{k,y} &= \frac{y_{\mathrm{TX},k} - y_0}{\sqrt{(x_{\mathrm{TX},k} - x_0)^2 + \left(y_{\mathrm{TX},k} - y_0\right)^2 + (z_{\mathrm{TX},k} - z_0)^2}} + \frac{y_0}{\sqrt{x_0^2 + y_0^2 + z_0^2}} \\ a_{k,z} &= \frac{z_{\mathrm{TX},k} - z_0}{\sqrt{(x_{\mathrm{TX},k} - x_0)^2 + \left(y_{\mathrm{TX},k} - y_0\right)^2 + (z_{\mathrm{TX},k} - z_0)^2}} + \frac{z_0}{\sqrt{x_0^2 + y_0^2 + z_0^2}} \end{aligned} \tag{12}$$

In matrix notation this equals:

$$\boldsymbol{A\delta} = \boldsymbol{b}$$
$$\boldsymbol{A} = \begin{bmatrix} a_{1,x} & a_{1,y} & a_{1,z} \\ a_{2,x} & a_{2,y} & a_{2,z} \\ \vdots & \vdots & \vdots \\ a_{k,x} & a_{k,y} & a_{k,z} \end{bmatrix} \qquad \boldsymbol{\delta} = \begin{bmatrix} \delta_x \\ \delta_y \\ \delta_z \end{bmatrix} \qquad \boldsymbol{b} = \begin{bmatrix} d_1 - \boldsymbol{R}_{\mathrm{bi},1} \\ d_2 - \boldsymbol{R}_{\mathrm{bi},2} \\ \vdots \\ d_k - \boldsymbol{R}_{\mathrm{bi,k}} \end{bmatrix} \tag{13}$$

where matrix $\boldsymbol{A}$ represents the geometry matrix or Jacobian matrix containing the partial derivatives for the variables. The vector $\boldsymbol{\delta}$ contains the three-dimensional error components for the object position estimation. Additionally, vector $\boldsymbol{b}$ is the calculated difference between the measured length of the reflection path d_i and the function value at the estimated object position $\boldsymbol{R}_{\mathrm{bi,k}}(x_0, y_0, z_0)$. The linear equation system can then be solved using the least squares approach [38]:

$$\boldsymbol{\delta} = \left(\boldsymbol{A}^{\intercal}\boldsymbol{A}\right)^{-1}\boldsymbol{A}^{\intercal}\boldsymbol{b} \tag{14}$$

The calculated residual of the position estimation $\boldsymbol{\delta}$ is used to adjust the estimation (Eq. (15)), which is also the starting point for the next iteration of the method:

$$x_0 \leftarrow x_0 - \delta_x, \qquad y_0 \leftarrow y_0 - \delta_y, \qquad z_0 \leftarrow z_0 - \delta_z \tag{15}$$

4.3 Theoretical bounds and geometric dilution of precision

To assess the influence of the geometric constellation between network nodes and scatter points the Cramer-Rao lower bound (CRLB) is computed. The CRLB is the theoretical limit on the performance and accuracy (error variance) of any unbiased estimator and can be derived by the inverse of the Fisher information matrix (FIM). If the FIM is positive definite or non-singular, then the inverse of $\boldsymbol{J}$ exists and the CRLB can be written as [43]:

$$CRLB = \boldsymbol{J}^{-1} \tag{16}$$

The geometric dilution of precision (GDOP) is the ratio of the accuracy limitation of the localization to the accuracy of measurements and is calculated based on the CRLB as follows [44]:

$$GDOP = \sqrt{\mathrm{tr}(CRLB)} = \sqrt{\mathrm{tr}\left(\boldsymbol{J}^{-1}\right)} \tag{17}$$

where $\mathrm{tr}(\cdot)$ donates to the trace of the square matrix of CRLB. If all measurement errors are to be considered zero-mean independent and identically distributed Gaussian variables in the positioning system the GDOP is [45]:

$$GDOP = \sqrt{\mathrm{tr}\left(\boldsymbol{A}^T\boldsymbol{A}\right)^{-1}} \tag{18}$$

where $\boldsymbol{A}$ represents the Jacobian matrix as in Eq. (12).

The CRLB of the positioning accuracy depends also on the ranging error or error in the MPC extraction [46]. This error also results partly from the limits in the range resolution of UWB (Section 3.4).

Figure 7 presents the calculated GDOP map for every possible target position inside a grid around the sensors for two different sensor arrangements. The GDOP is calculated following Eq. (18) based on the Jacobian matrix $\boldsymbol{A}$ in Eq. (13) for position candidates represented by an equidistant grid. The resulting GDOPs are indicated by the color scale. The first geometric constellation has some areas with degraded GDOP values, while the second symmetrical sensor arrangement around the target results in lower GDOP values and thus a better accuracy [43].

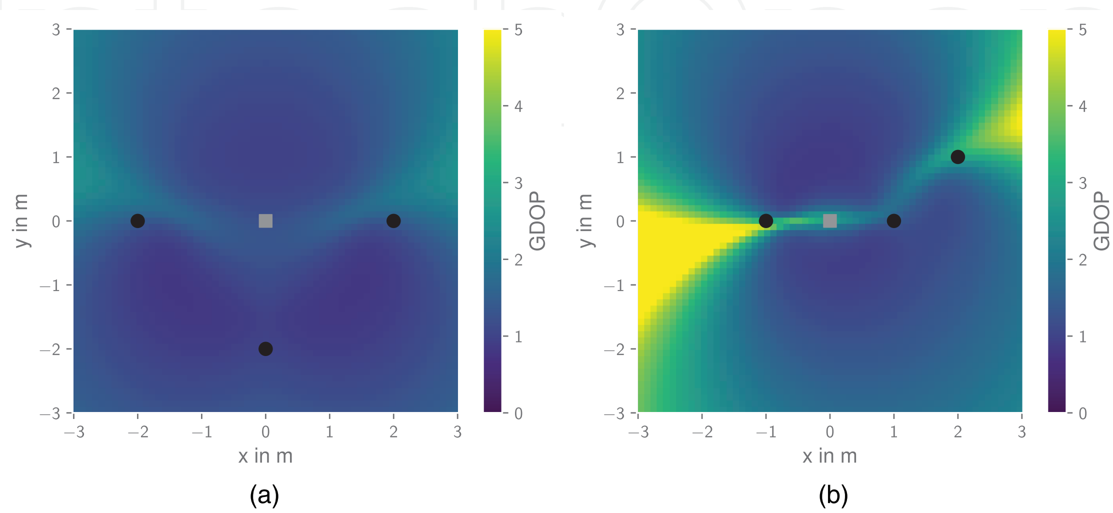

Figure 7.
GDOP map for localization with two different sensor constellations with three TX (black) and one RX (gray). The GDOP (color scale) is calculated for each target position within an equidistant grid sampled with 0.1 m.

4.4 Tasks and functionalities of radio sensing

Radio sensing fulfills different tasks and functionalities depending on the use case (cf. **Table 1**). These tasks include but are not limited to localization, tracking, mapping/imaging, presence detection, counting, or classification and are enabled by specific algorithms. The data processing to achieve the different sensing tasks concerning to UWB specifics is outlined in **Figure 8**. The input for all UWB radio sensing tasks and functionalities is the CIR, from which the clutter is removed beforehand (Section 5.2). Mapping, classification, and counting use all values in the CIR, whereas detection and localization are based on the extracted MPC at the target object.

Figure 9 depicts a collection of results of algorithms and methods to enable radio sensing. All subfigures show original content and were created based on the frameworks and algorithms detailed in [47–49]. The software used to create the illustrations is indicated on the backmatter.

The goal of passive localization is to estimate the position of the target object in a multistatic sensor network based on the measured bistatic ranges between multiple TX and RX. The bistatic range corresponds to the length of the reflection path and can be estimated as MPC from the CIR. An ellipse is defined by the constant bistatic range, on which the target lies, with its foci being located at the TX and RX positions. The target position can either be estimated by setting up the ellipse equation and calculating the intersections of these ellipses or by solving the non-linear equation system (9) with a Taylor series linearization as outlined in Section 4.2. **Figure 9a** shows the localization with the elliptical model with four sensors (three TX and one RX) and the target at the intersection point of the ellipses [42].

Mapping or imaging is accomplished by using the whole CIRs obtained between all TX and the RX. For that, a single CIR is spatially mapped based on the elliptical model resulting in a crowd of ellipses for every distance value in the CIR with the corresponding amplitude values as magnitude. After interpolating the ellipses and combining the resulting grid with the other mapped CIRs in the sensor network, a heatmap of the environment is obtained. The heatmap in **Figure 9b** highlights regions with reflections at the target objects in yellow. The map could also be used to estimate the position of the target objects or even multiple objects [47].

The next task for sensing is the detection of objects or even counting multiple objects/people. Detection is achieved by only analyzing the CIR. As shown in

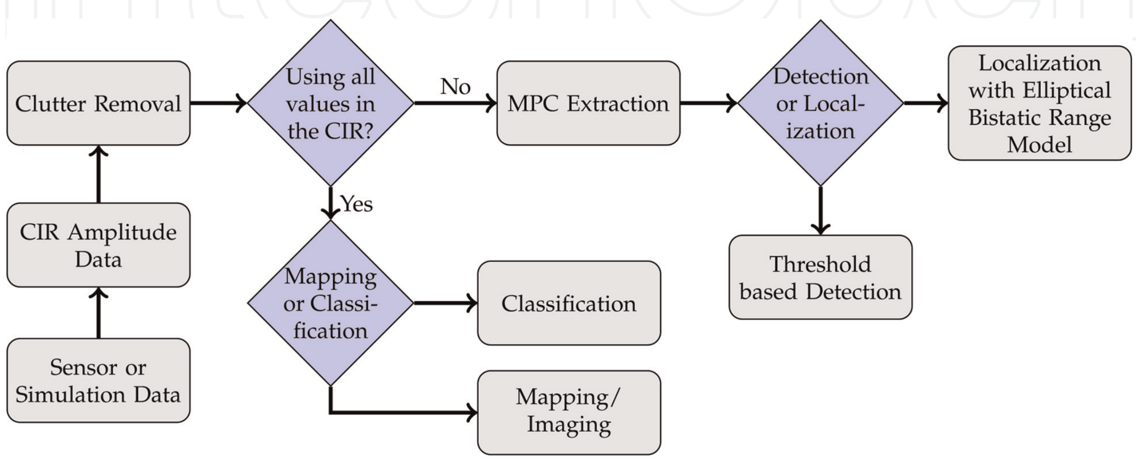

Figure 8.
The connection between data processing and the various sensing tasks.

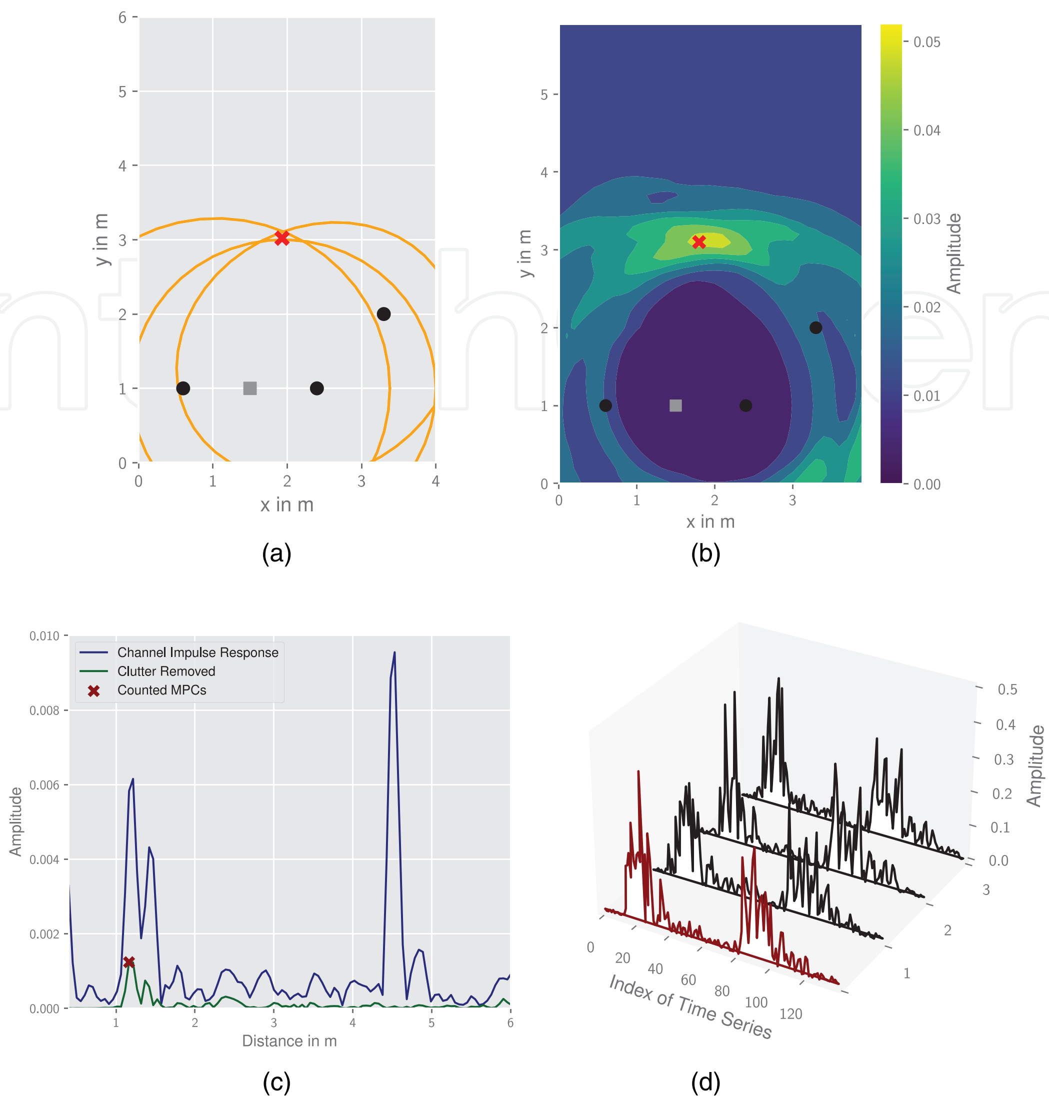

Figure 9.
Tasks of radio sensing: (a) localization with elliptical model, (b) mapping and imaging, (c) detecting and counting with MPC extraction, (d) classification of CIRs with k-nearest neighbor (kNN) algorithm.

Figure 9c, the CIR is filtered to remove the static background using the reference method described in Section 5.2. Then, the MPC from the wanted target is extracted using a simple threshold detector [48]. Further challenges for clutter removal and MPC extraction are discussed in Section 5.2. The CIR and extraction of MPCs could also be used for counting objects or people. Here, the different peaks and local maxima in the CIR are clustered, probability filtered, and the number of targets are extracted by a maximum likelihood estimator [26].

The whole CIR is used for classification for example based on the k-nearest neighbor (kNN) algorithm to distinguish between different states. Therefore, the test data is compared with pre-recorded training data by finding the minimum distance determined by a specific metric. Thus, the recorded CIR could be assigned to a state/class for example to derive a detection status. **Figure 9d** shows an assembled time series from two measured CIRs of the test dataset (red) compared to the three closest time series of the training dataset (black). The kNN algorithm uses a Euclidean metric and the three closest neighbors in the training dataset to determine the state/class of the test sample. The example in **Figure 9d** shows the measured data from seat occupancy detection inside a connected aircraft cabin using UWB. The static background from the CIR is removed beforehand and the CIRs from the different sensors are combined into a unified time series [49].

5. Challenges and research directions

In this section, selected challenges for UWB-based radio sensing are discussed and further research directions are derived. Since the focus in this chapter is on transport and mobility, the challenges are mainly highlighted based on the various use cases in this area.

5.1 Performance indicators and metrics

Moving from solely communication purposes toward perceptive networks fundamentally changes how wireless systems are evaluated. State-of-the-art performance metrics, such as the received signal strength (RSS) or signal-to-interference-plus-noise ratio (SINR), are not useful to evaluate radio sensing systems. Instead, specific metrics for different sensing tasks from other research domains should be applied. For example, vision technologies, such as LiDAR and camera commonly uses the probability of detection [50] to determine the detectability of objects, IPS apply the root mean square error (RMSE) as an accuracy metric, or classification tasks consider the accuracy to predict the label of an object. To further elaborate, **Table 3** proposes and briefly describes performance metrics for different sensing tasks. One challenge is to select the right metric for the desired task and to combine and weigh different metrics.

5.2 Clutter removal and MPC extraction

Clutter is MPCs from the static background environment. In general, these signals are not of interest for sensing applications, but instead only the reflected signals from the target object or detected people need to be considered. The task of clutter removal is to remove or suppress these MPCs in the CIR. One approach is the background subtraction of multipath signals originating from permanent or long-period static objects. There are two methods for background subtraction: the reference method and the dynamic method [5, 7, 51].

The reference method subtracts an averaged reference signal $\overline{h}^{\mathrm{ref}}(t)$ without the target object from the measurement with the target object $h(t)$ flowing Eq. (19). This

Task	Metrics	Description
Localization	Accuracy, mean absolute error (MAE), RMSE	Euclidean distance between estimated position and true position
Tracking	Empirical cumulative distribution functions (ECDF)	MAE or RMSE over the track
Detection	Probability of detection, SINR, prominence, isolation [50]	
Classification	Accuracy, confusion matrix	Confusion matrix to compare predicted and actual class

Table 3.
Possible performance indicators and metrics for different sensing tasks.

method is best suited for static environments and when the calibration with the reference signal is possible beforehand [7, 50]:

$$\overline{h}^{\text{sub}}(t) = |h(t) - \overline{h}^{\text{ref}}(t)| \tag{19}$$

The dynamic method subtracts the static, time-invariant background based on exponential averaging. The background b_t is computed using the previous background estimate b_{t-1} and the newly received CIR h_t [52]:

$$b_t = \alpha b_{t-1} + (1-\alpha)h_t \tag{20}$$

The constant scalar weighing factor α between 0 and 1 determines whether recent or long-term events are emphasized. The clutter-removed signal $\overline{h}^{\text{sub}}(t)$ is then also obtained by subtraction:

$$\overline{h}^{\text{sub}}(t) = |h_t - b_t| \tag{21}$$

In non-stationary scenarios, clutter removal is much harder, especially in dynamic environments, and can lead to missed detection of the target during the measurement time. Also, background subtraction is not effective in dense multipath scenarios [25].

In addition, the extraction of the MPC with the corresponding time delay from the CIR is of upmost importance to fulfill the different sensing tasks. First, a basic maximum or threshold detector could be used to find the MPC peak in the CIR. More advanced methods cluster the different peaks in the CIR to MPC clusters, which are from a single target object. Other methods used for UWB signals for MPC extraction are detectors of distributed targets (so-called (N,k)-detector), the interperiod-correlation processing (IPCP) detector, and the constant false alarm rate (CFAR) detector [53].

Froehle [36] uses an MPC extraction algorithm consisting of three steps to tackle this challenge. First, all peaks in the CIR are searched with a high-resolution peak search, then a weighting factor is applied before the estimated MPC is detected and canceled out as the strongest scatter. This process is repeated for more attenuated scatter and MPCs [36].

The precondition for the MPC extraction and delay estimation is the distinctness of the MPCs in the CIR. This is especially challenging when the reflected signal strength from a long propagation path is very weak, the target is hidden or shadowed behind other objects, or the MPCs could not be isolated due to limited range resolution and bandwidth [25, 47].

5.3 Channel model and propagation simulation

Commonly the channel for communication systems is modeled with empirical or statistical models like the 3GPP TR 38.901 for 5G [33]. These models are based on measurements of channel statistics for different predefined environment categories such as indoor, urban, or rural. In comparison, deterministic channel models like the multipath channel model described in Section 3 use individual propagation paths or rays as a modeling foundation. This approach is generally suitable for sensing approaches and applications because every ray and MPC can individually be modeled.

Often ray tracing is used to calculate the delay of every propagation path or ray. In addition, the attenuation of the path is determined taking FSPL, reflection, scattering, and diffraction losses into account. Ray tracing is a computationally intensive operation and much more complex than statistical models [54].

An example of a radio sensing mapping task is to estimate the occupancy state of a parking lot in a car park for smart parking and ticketing, as depicted in **Figure 10**. The car park environment is geometrically modeled, and the material properties are applied. Sensors are deployed at different locations (**Figure 10a**), and the signal parameters are complying with UWB [54]. The center frequency is set to 6.5 GHz and the transmit power to -41.3 dBm MHz^{-1}. Then, the individual propagation paths with their corresponding received signal power and propagation delay are computed with the radio propagation simulation software *Altair Feko/WinProp 2022* [55] using the deterministic ray tracing model (**Figure 10a**). After the simulation, the propagation delays and amplitudes are used to obtain the bandlimited reconstructed CIR with help of Eq. (6) in a custom software framework. Since the simulation is performed without and with the target vehicle, the static background subtraction is applied based on the

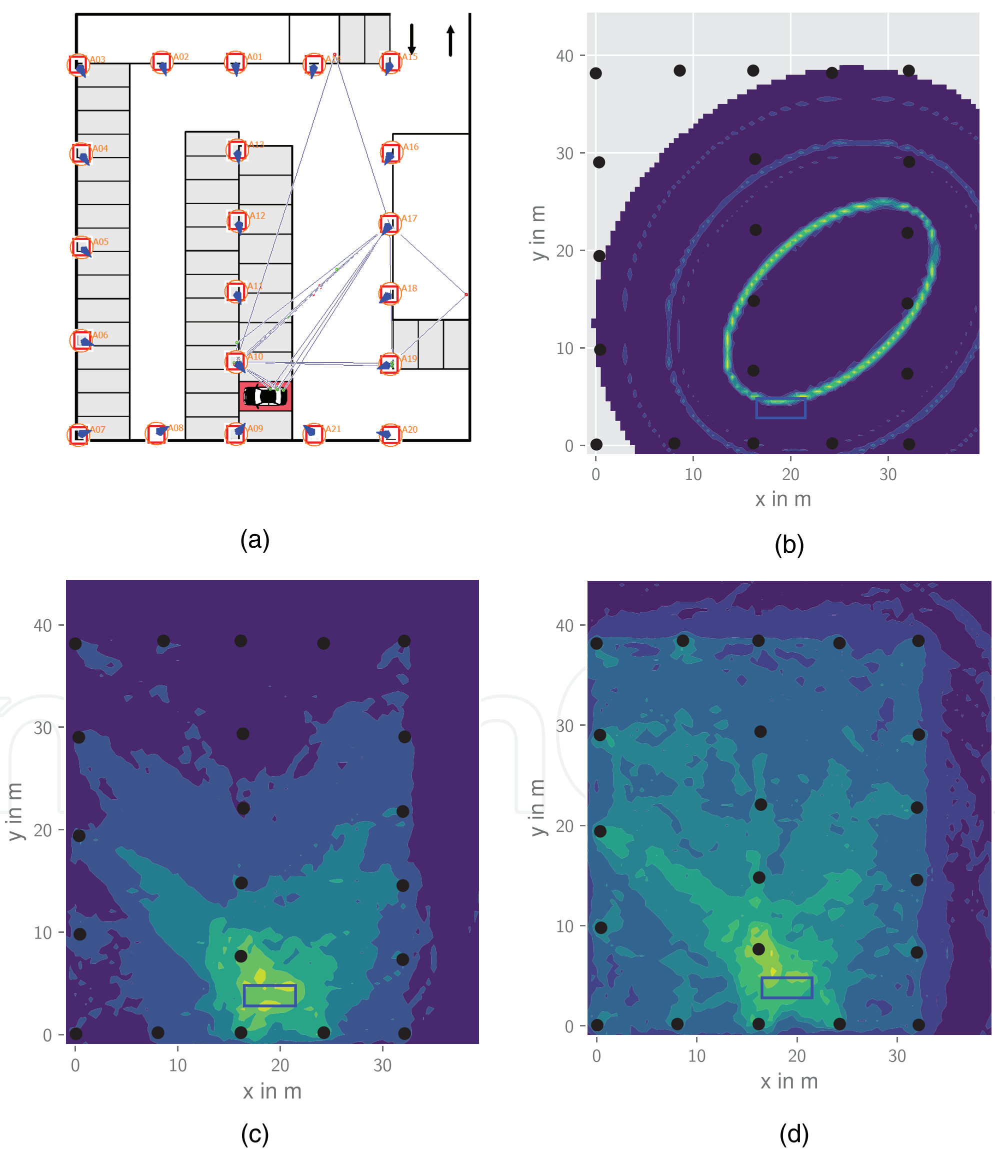

Figure 10.
Antenna comparison for a radio sensing application: (a) radio propagation simulation with Altair Feko/WinProp 2022 [55] for parking plot occupancy detection in a car park with an example of computed rays between two sensors, (b) mapping of a CIR between two sensors (black circles) as a family of ellipses, resulting interpolated heatmap with (c) omnidirectional antennas and (d) directional/sector antennas.

reference method described in Section 5.2. The subtracted CIRs between all sensors are mapped with the elliptical method described in Section 4.4 (**Figure 10b**). Interpolating and combining the maps of all sensor combinations results in a heatmap of the environment highlighting the reflections of the target object for two different antenna configurations (**Figure 10c** and d) [56].

In the future, a combination of deterministic ray tracing and statistical models will be needed to evaluate integrated communication systems with both data transmission and radio sensing capabilities [18].

5.4 Directional antennas

The sensing performance can not only be enhanced with enhanced signal processing but also directly by antennas and the HF signal itself. Omnidirectional antennas radiate the radio power in all directions perpendicular to the azimuth directions equality, whereas specific directional antennas have much higher antenna gain in a specific direction. This means that the signal from this direction is amplified, whereas signals from other directions are much more attenuated. In terms of radio sensing, the reflected signal strength from the desired direction is much stronger in the CIR, so the MPC can be isolated more accurately to find the position of the target. In addition, sector antennas combine multiple directional antenna elements and are switchable to a desired sector and direction. Beamforming even allows spatial selectivity of an antenna array by dynamically controlling the phase and relative amplitude of the signal.

To investigate the influence of directional antennas on the sensing performance, the radio propagation simulation based on ray tracing with *Altair Feko/WinProp 2022* [55] can be used. **Figure 10** compares the mapping/imaging of a car park to estimate the occupancy state of a parking lot with omnidirectional antennas against directional antennas. Due to the selectivity of the antenna and the antenna gain in direction of the target vehicle, reflections are much stronger and highlighted at the boundaries of the vehicle from all sites.

The antenna choice directly affects the radio sensing performance and should be further investigated and considered in addition to algorithms and signal processing improvements.

6. Conclusions

The main contribution of this chapter is the transfer of UWB IR to the emerging research field of radio sensing from a mobility and transportation applications perspective. Therefore, the wideband multipath channel model was introduced and the theoretical bounds for range resolution and GDOP were concluded. Different tasks and functionalities of radio sensing were described across the board ranging from detection, localization, mapping/imaging, counting, and classification. The approaches and algorithms are promising and allow a wide range of use cases of radio sensing in ITS overall modes of transport, for example, smart parking and ticketing, connected aircraft cabin or vehicular networks, and automotive radar.

However, some challenges need to be addressed in further research to implement UWB-based radio sensing systems in real-world applications. These include adaptability to the environment, scalability to a larger sensor network and reliability and robustness of the discussed approaches and algorithms. One approach is machine learning (ML) algorithms to classify the different detection states. This does not require prior MPC extraction. Instead, the entire CIR is used to train and test the classifier with predefined detection scenes and labels to improve the robustness of the detection. Another promising research direction is the integration of radio sensing into a UWB RTLS system to improve the integrity of the localization and enable detection or localization when the object does not carry an active sensor. A fully integrated solution may also use a SLAM approach for anchor mapping, active mobile tag localization, and radio sensing for detection and other tasks.

Software

All calculations, algorithms, and plotting of figures were performed with Python (version 3.10) [57] using the following additional packages: matplotlib (3.6.2) [58], numpy (1.22.4) [59], and scipy (1.9.0) [60]. The radio propagation simulation is carried out with Altair Feko/WinProp 2022 [55].

Author details

Jonas Ninnemann*†, Paul Schwarzbach† and Oliver Michler
Transport Systems Information Technology, Institute of Traffic Telematics, Technische Universität Dresden, Dresden, Germany

*Address all correspondence to: jonas.ninnemann@tu-dresden.de

† These authors contributed equally.

References

[1] Zafari F, Gkelias A, Leung KK. A survey of indoor localization systems and technologies. IEEE Communications Surveys & Tutorials. 2019;**21**(3):2568-2599. DOI: 10.1109/COMST.2019.2911558

[2] Shi G, Ming Y. Survey of indoor positioning systems based on ultra-wideband (UWB) technology. In: Zeng QA, editor. Wireless Communications, Networking and Applications. Lecture Notes in Electrical Engineering. India: Springer; 2016. pp. 1269-1278. DOI: 10.1007/978-81-322-2580-5_115

[3] Lee G, Park J, Jang J, Jung T, Kim TW. An IR-UWB CMOS transceiver for high-data-rate, low-power, and short-range communication. IEEE Journal of Solid-State Circuits. 2019;**54**(8):2163-2174. DOI: 10.1109/JSSC.2019.2914584

[4] Barneto CB, Turunen M, Liyanaarachchi SD, Anttila L, Brihuega A, Riihonen T, et al. High-accuracy radio sensing in 5G new radio networks: Prospects and self-interference challenge. In: 53rd Asilomar Conference on Signals, Systems, and Computers; 03–06 November 2019. Vol. 2019. Pacific Grove, CA, USA: IEEE; 2019. pp. 1159-1163. DOI: 10.1109/IEEECONF44664.2019.9048786

[5] Zhang JA, Rahman ML, Wu K, Huang X, Guo YJ, Chen S, et al. Enabling joint communication and radar sensing in Mobile networks -a survey. IEEE Communications Surveys Tutorials. 2021;**24**(1):306-345. DOI: 10.1109/COMST.2021.3122519

[6] Chen Y, Zhang J, Feng W, Alouini MS. Radio sensing using 5G signals: Concepts, state of the art, and challenges. IEEE Internet of Things Journal. 2022;**9**(2):1037-1052. DOI: 10.1109/JIOT.2021.3132494

[7] Ledergerber A, D'Andrea R. A multi-static radar network with ultra-wideband radio-equipped devices. Sensors. 2020;**20**(6):1599. DOI: 10.3390/s20061599

[8] Dong J, Guo Q, Liang X. Through-Wall moving target tracking algorithm in multipath using UWB radar. IEEE Geoscience and Remote Sensing Letters. 2021;**19**:3503405. DOI: 10.1109/lgrs.2021.3050501

[9] Le C, Dogaru T, Nguyen L, Ressler MA. Ultrawideband (UWB) radar imaging of building interior: Measurements and predictions. IEEE Transactions on Geoscience and Remote Sensing. 2009;**47**(5):1409-1420. DOI: 10.1109/TGRS.2009.2016653

[10] Choi JH, Kim JE, Kim KT. People counting using IR-UWB radar sensor in a wide area. IEEE Internet of Things Journal. 2021;**8**(7):5806-5821. DOI: 10.1109/JIOT.2020.3032710

[11] Cimdins M, Schmidt SO, Bartmann P, Hellbrück H. Exploiting ultra-Wideband Channel impulse responses for device-free localization. Sensors. 2022;**22**(16):6255. DOI: 10.3390/s22166255

[12] Goldsmith A. Wireless Communications. Cambridge: Cambridge University Press; 2005. pp. 27-98. DOI: 10.1017/CBO9780511841224

[13] Tse D, Viswanath P. Fundamentals of Wireless Communication. Cambridge: Cambridge University Press; 2005. pp. 10-48. DOI: 10.1017/CBO9780511807213

[14] Youssef M, Mah M, Agrawala A. Challenges: Device-free passive localization for wireless environments. In: Proceedings of the 13th Annual ACM International Conference on Mobile Computing and Networking - MobiCom '07. September 2007. Montréal, Québec, Canada: ACM Press; 2007. pp. 222-229. DOI: 10.1145/1287853.1287880

[15] Jovanoska S, Zetik R, Thoma R, Govaers F, Wilds K, Koch W. Device-free indoor localization using a distributed network of autonomous UWB sensor nodes. In: 2013 Workshop on Sensor Data Fusion: Trends, Solutions, Applications (SDF); 09–11 October 2013. Bonn, Germany: IEEE; 2013. pp. 1-6. DOI: 10.1109/SDF.2013.6698264

[16] Mahafza BR, Winton SC, Elsherbeni AZ. Handbook of Radar Signal Analysis. Boca Raton, US: CRC Press; 2021. pp. 93-126

[17] Liu F, Cui Y, Masouros C, Xu J, Han TX, Eldar YC, et al. Integrated sensing and communications: Towards dual-functional wireless networks for 6G and beyond. IEEE Journal on Selected Areas in Communications. 2022;**40**(6): 1728-1767. DOI: 10.1109/JSAC.2022.3156632

[18] Wild T, Braun V, Viswanathan H. Joint Design of Communication and Sensing for beyond 5G and 6G systems. IEEE Access. 2021;**9**:30845-30857. DOI: 10.1109/access.2021.3059488

[19] Cimdins M, Schmidt SO, Hellbrück H. MAMPI-UWB—Multipath-assisted device-free localization with magnitude and phase information with UWB transceivers. Sensors. 2020;**20**(24):7090. DOI: 10.3390/s20247090

[20] Schmidhammer M, Siebler B, Gentner C, Sand S, Fiebig UC. Bayesian multipath-enhanced device-free localisation: Simulation-and measurement-based evaluation. IET Microwaves, Antennas & Propagation. 2022;**16**(6):327-337. DOI: 10.1049/mia2.12244

[21] Gentner C, Jost T, Wang W, Zhang S, Dammann A, Fiebig UC. Multipath assisted positioning with simultaneous localization and mapping. IEEE Transactions on Wireless Communications. 2016;**15**(9):6104-6117. DOI: 10.1109/TWC.2016.2578336

[22] Bocus MJ, Piechocki R. A comprehensive ultra-wideband dataset for non-cooperative contextual sensing. Scientific Data. 2022;**9**(1):650. DOI: 10.1038/s41597-022-01776-7

[23] Leitinger E, Meissner P, Rüdisser C, Dumphart G, Witrisal K. Evaluation of position-related information in multipath components for indoor positioning. IEEE Journal on Selected Areas in Communications. 2015;**33**(11): 2313-2328. DOI: 10.1109/JSAC.2015.2430520

[24] Froehle M, Meissner P, Witrisal K. Tracking of UWB multipath components using probability hypothesis density filters. In: 2012 IEEE International Conference on Ultra-Wideband; 17–20 September 2012. Syracuse, NY, USA: IEEE; 2012. pp. 306-310. DOI: 10.1109/ICUWB.2012.6340452

[25] Li C, Tanghe E, Fontaine J, Martens L, Romme J, Singh G, et al. Multi-static UWB radar-based passive human tracking using COTS devices. IEEE Antennas and Wireless Propagation Letters. 2022;**21**(4):695-699. DOI: 10.1109/LAWP.2022.3141869

[26] Choi JW, Yim DH, Cho SH. People counting based on an IR-UWB radar sensor. IEEE Sensors Journal. 2017;

17(17):5717-5727. DOI: 10.1109/JSEN.2017.2723766

[27] Qorvo. DW1000 – Qorvo. 2022. Available from: https://www.qorvo.com/products/p/DW1000

[28] Friis HT. A note on a simple transmission formula. Proceedings of the IRE. 1946;**34**(5):254-256. DOI: 10.1109/JRPROC.1946.234568

[29] Kim H. Wireless Communications Systems Design. Chichester, West Sussex. United Kingdom: John Wiley & Sons, Ltd; 2016. pp. 32-51

[30] Pätzold M. Mobile Radio Channels. Chichester, West Sussex. United Kingdom: John Wiley & Sons, Ltd; 2011. pp. 338-342

[31] Hari KVS. Channel models for wireless communication systems. In: Kennington J, Olinick E, Rajan D, editors. Wireless Network Design: Optimization Models and Solution Procedures. International Series in Operations Research & Management Science. New York, NY: Springer; 2011. pp. 47-64. DOI: 10.1007/978-1-4419-6111-2_3

[32] Molisch AF. Ultra-wide-band propagation channels. Proceedings of the IEEE. 2009;**97**(2):353-371. DOI: 10.1109/JPROC.2008.2008836

[33] 3GPP Radio Access Network Working Group. Study on channel model for frequencies from 0.5 to 100 GHz (Release 16). Vol. 16. 3GPP TR 38.901; 2020

[34] Ulmschneider M. Cooperative Multipath Assisted Positioning [Ph.D. thesis]. Hamburg, Germany: Technischen Universität Hamburg; 2021. DOI: 10.15480/882.3299

[35] Wang Z, Han K, Shen X, Yuan W, Liu F. Achieving the performance bounds for sensing and Communications in Perceptive Networks: Optimal bandwidth allocation. IEEE Wireless Communications Letters. September 2022; **11**(9):1835-1839. DOI: 10.1109/LWC.2022.3183235

[36] Froehle M, Meissner P, Gigl T, Witrisal K. Scatterer and virtual source detection for indoor UWB channels. In: 2011 IEEE International Conference on Ultra-Wideband (ICUWB); 14–16 September 2011. Bologna, Italy: IEEE; 2011. pp. 16-20. DOI: 10.1109/ICUWB.2011.6058819

[37] Malanowski M, Kulpa K. Two methods for target localization in multistatic passive radar. IEEE Transactions on Aerospace and Electronic Systems. 2012;**48**(1):572-580. DOI: 10.1109/TAES.2012.6129656

[38] Zaied S. UWB Localization of People - Accuracy Aspects. [Master Thesis]. Ilmenau, Germany: Ilmenau University of Technology; 2009

[39] Noroozi A, Sebt MA. Comparison between range-difference-based and Bistatic-range-based localization in multistatic passive radar. In: 2015 16th International Radar Symposium (IRS); 24–26 June 2015. Dresden, Germany: IEEE; 2015. pp. 1058-1063. DOI: 10.1109/IRS.2015.7226218

[40] Smith J, Abel J. Closed-form least-squares source location estimation from range-difference measurements. IEEE Transactions on Acoustics, Speech, and Signal Processing. 1987;**35**(12):1661-1669. DOI: 10.1109/TASSP.1987.1165089

[41] Mellen G, Pachter M, Raquet J. Closed-form solution for determining emitter location using time difference of arrival measurements. IEEE

Transactions on Aerospace and Electronic Systems. 2003;**39**(3): 1056-1058. DOI: 10.1109/ TAES.2003.1238756

[42] Kocur D, Švecová M, Rovňáková J. Through-The-Wall localization of a moving target by two independent ultra wideband (UWB) radar systems. Sensors. 2013;**13**(9):11969-11997. DOI: 10.3390/s130911969

[43] Godrich H, Haimovich AM, Blum RS. Cramer Rao bound on target localization estimation in MIMO radar systems. In: 2008 42nd Annual Conference on Information Sciences and Systems; 19–21 March 2008. Princeton, NJ, USA: IEEE; 2008. pp. 134-139. DOI: 10.1109/CISS.2008.4558509

[44] Zhang J, Lu J. Analytical evaluation of geometric dilution of precision for three-dimensional angle-of-arrival target localization in wireless sensor networks. International Journal of Distributed Sensor Networks. 2020;**16**(5):1-14. DOI: 10.1177/ 1550147720920471

[45] Lv X, Liu K, Hu P. Geometry influence on GDOP in TOA and AOA positioning systems. In: 2010 Second International Conference on Networks Security, Wireless Communications and Trusted Computing. Vol. 2. Wuhan, China: IEEE; 2010. pp. 58-61. DOI: 10.1109/NSWCTC.2010.150

[46] Jing H, Pinchin J, Hill C, Moore T. An adaptive weighting based on modified DOP for collaborative indoor positioning. The Journal of Navigation. 2016;**69**(2):225-245. DOI: 10.1017/ S037346331500065X

[47] Ninnemann J, Schwarzbach P, Jung A, Michler O. Lab-based evaluation of device-free passive localization using Multipath Channel information. Sensors. 2021;**21**(7):2383. DOI: 10.3390/ s21072383

[48] Ninnemann J, Schwarzbach P, Michler O. Multipath-assisted radio sensing and occupancy detection for smart in-house parking in ITS. In: WiP Proceedings of the Eleventh International Conference on Indoor Positioning and Indoor Navigation - Work-in-Progress Papers (IPIN-WiP 2021); 29 November - 02 December 2021. Lloret de Mar, Spain: CEUR-WS; 2021. pp. 1-15. DOI: 10.48550/ arXiv.2201.06128

[49] Ninnemann J, Schwarzbach P, Schultz M, Michler O. Multipath-assisted radio sensing and state detection for the connected aircraft cabin. Sensors. 2022; **22**(8):2859. DOI: 10.3390/s22082859

[50] Arnold M, Bauhofer M, Mandelli S, Henninger M, Schaich F, Wild T, et al. MaxRay: A raytracing-based integrated sensing and communication framework. In: 2022 2nd IEEE International Symposium on Joint Communications & Sensing (JC&S); 09–10 March 2022. Seefeld, Austria: IEEE; 2022. pp. 1-7. DOI: 10.1109/JCS54387.2022.9743510

[51] Shaikh SH, Saeed K, Chaki N. Moving Object Detection Using Background Subtraction. SpringerBriefs in Computer Science. Cham, Germany: Springer International Publishing; 2014. pp. 15-16. DOI: 10.1007/978-3- 319-07386-6_3

[52] Jovanoska S, Thomä R. Multiple target tracking by a distributed UWB sensor network based on the PHD filter. In: 2012 15th International Conference on Information Fusion; 09–12 July 2012. Singapore: IEEE; 2012. pp. 1095-1102

[53] Rovnakova J, Svecova M, Kocur D, Nguyen TT, Sachs J. Signal processing for through wall moving target tracking by

M-sequence UWB radar. In: 2008 18th International Conference Radioelektronika; 24–25 April 2008. Prague, Czech Republic: IEEE; 2008. pp. 1-4. DOI: 10.1109/RADIOELEK.2008. 4542694

[54] Ußler H, Porepp K, Ninnemann J, Schwarzbach P, Michler O. Demo: Deterministic radio propagation simulation for integrated communication Systems in Multimodal Intelligent Transportation Scenarios. In: 2022 IEEE International Conference on Communications Workshops (ICC Workshops); 16–20 May 2022. Seoul, Republic of Korea: IEEE; 2022. pp. 1-2. DOI: 10.1109/ICCWorkshops53468. 2022.9915017

[55] Altair Engineering Inc. Altair Feko Applications [Internet]. 2022. Available from: https://www.altair.com/feko-applications [Accessed: April 1, 2023]

[56] Schwarzbach P, Ninnemann J, Michler O. Enabling radio sensing for multimodal intelligent transportation systems: From virtual testing to immersive testbeds. In: 2022 2nd IEEE International Symposium on Joint Communications & Sensing (JC&S); 09–10 March 2022. Seefeld, Austria: IEEE; 2022. pp. 1-6. DOI: 10.1109/JCS54387.2022.9743504

[57] Van Rossum G, Drake FL. Python 3 Reference Manual. Scotts Valley, CA: CreateSpace; 2009

[58] Hunter JD. Matplotlib: A 2D graphics environment computing in science & engineering. Mai. 2007;**9**(3):90-95. DOI: 10.1109/MCSE.2007.55

[59] Harris CR, Millman KJ, van der Walt SJ, Gommers R, Virtanen P, Cournapeau D, et al. ’ Array programming with NumPy. Nature. 2020;**585**(7825):357-362. DOI: 10.1038/s41586-020-2649-2

[60] Virtanen P, Gommers R, Oliphant TE, Haberland M, Reddy T, Cournapeau D, et al. SciPy 1.0: Fundamental algorithms for scientific computing in python. Nature Methods. 2020;**17**(3):261-272. DOI: 10.1038/s41592-019-0686-2